

Linear diffraction grating interferometer with high alignment tolerance and high accuracy

Fang Cheng^{1,2} and Kuang-Chao Fan^{2,3,*}

¹School of Mechanical & Aerospace Engineering, Nanyang Technological University, 639798, Singapore

²School of Instrument Science and Optoelectronics Engineering, Hefei University of Technology, Hefei, Anhui, 230009, China

³Department of Mechanical Engineering, National Taiwan University, Taipei, 10617, Taiwan

*Corresponding author: fan@ntu.edu.tw

Received 29 April 2011; accepted 9 June 2011;
posted 16 June 2011 (Doc. ID 144988); published 29 July 2011

We present an innovative structure of a linear diffraction grating interferometer as a long stroke and nanometer resolution displacement sensor for any linear stage. The principle of this diffractive interferometer is based on the phase information encoded by the ± 1 st order beams diffracted by a holographic grating. Properly interfering these two beams leads to modulation similar to a Doppler frequency shift that can be translated to displacement measurements via phase decoding. A self-compensation structure is developed to improve the alignment tolerance. LightTool analysis shows that this new structure is completely immune to alignment errors of offset, standoff, yaw, and roll. The tolerance of the pitch is also acceptable for most installation conditions. In order to compact the structure and improve the signal quality, a new optical bonding technology by mechanical fixture is presented so that the miniature optics can be permanently bonded together without an air gap in between. For the output waveform signals, a software module is developed for fast real-time pulse counting and phase subdivision. A laser interferometer HP5529A is employed to test the repeatability of the whole system. Experimental data show that within 15 mm travel length, the repeatability is within 15 nm. © 2011 Optical Society of America
OCIS codes: 050.1950, 120.3940, 120.3180.

1. Introduction

Optical instruments are widely used in length-scale measurement [1]. Solving the paradox between measuring range and resolution is challenging. A heterodyne phase detection laser interferometer is one of the most important noncontact metrology instruments for its high resolution and long measurement range, but it is expensive and sensitive to environmental conditions [2,3]. It is usually used as a calibrator, rather than a sensor, for precision linear stages. A homodyne intensity detection laser interferometer is simpler in structure, but is short in measurement range and also sensitive to its environment [4]. The other type of displacement sensor adopts the

pitch of a linear grating as the basic length unit, which is more insensitive to the environment [5]. Conventional moiré-type linear encoders have stable readings but the resolution is limited by the large grating pitch [1,6].

Grating interferometry is another approach for long-range nanomeasurement [7]. Fringe signals are generated by interfering with the laser beams diffracted by a nanoscale pitch grating [8]. With proper incident angles of the two input beams to the grating plane, the positive and negative diffraction beams of a certain order will propagate along the normal direction of the grating and the interference fringe will be detected by a photodetector or CCD [9,10]. Another method is to let the input beam be normal to the grating. Then the diffraction beams can be adjusted by mirrors and combined by a polarizing beam splitter (PBS) to form an interferogram [11–14].

0003-6935/11/224550-07\$15.00/0
© 2011 Optical Society of America

These methods, however, need rigorous positioning of the grating and the optical components. Although using higher orders of diffracted beams can obtain finer waveform pitch, signals become weak, yielding low signal-to-noise ratio. The signal quality will be notably affected by any tiny geometric error of the motion. In [15,16], a compact grating interferometer called a linear diffraction grating interferometer (LDGI) has been proposed by the authors. With certain incident angles, the ± 1 st order diffraction beams can propagate along the input paths, being a Littrow configuration, which has a higher tolerance of head-to-scale alignment errors. However, the system was influenced by unstable waveform distortions due to the process of adhesive bonding of miniature optical components.

Another technical issue in a nanometric grating interferometer is the method and algorithm for the waveform subdivision [17–19]. It is noted that output waveforms are not ideal quadrature signals. In [20], the typical signal distortions are analyzed and the corrective arithmetic is proposed. These signal distortions are mainly due to improper bondings of optical components. The current adhesive bonding method is subject to an air gap between two contacting surfaces and a gradual position shift during hardening. The more optical components, the more waveform distortions will be generated. The authors' group has developed signal correction and subdivision software [21], but for real-time measurements that system is still too slow.

In this paper, an improved design of an LDGI configuration is proposed. Compared with previous LDGI systems in [14,16,19], this system has the least number of optics, introduces an innovative mechanical clamping fixture for optical bonding of miniature components, and uses a robust and fast waveform correction and subdivision software. It is so compact that all components that are selected are 5 mm in size and the assembled module is only 40 mm by 40 mm in area. A real experimental test to 15 mm moving distance shows that this system can resist more geometrical tolerances with a positioning repeatability ($\pm 2\sigma$) below 15 nm and an average accuracy within 10 nm after a correction. Details are described in the following sections.

2. Principle of Compact LDGI

A. Structure of LDGI

The configuration of the proposed optical system is illustrated in Fig. 1. A partially polarized laser beam of 635 nm wavelength from the laser diode (LD) impinges on PBS1 and is split into two beams: the transmitted *P* beam and the reflected *S* beam. The intensity balance of these two beams can be adjusted by rotating the LD. Then both beams are directed by the mirrors M1 and M2–M3 onto the holographic gratings. With the incident angles equal to the $+1$ st and -1 st diffraction angles, respectively, from the left and right beams, the diffracted beams of

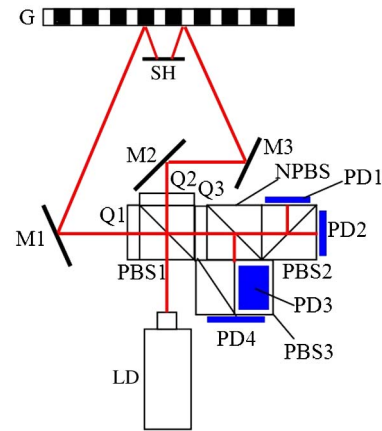


Fig. 1. (Color online) Improved design of LDGI (LD, laser diode; G, grating; SH, shield; PBSi, *i*th polarizing beam splitter; Mi, *i*th mirror; NPBS, nonpolarizing beam splitter; Qi, *i*th quarter-wave plate; PDi, *i*th photodetector).

the $+1$ st and -1 st order propagate along the same input paths, respectively. This is called the Littrow configuration of diffraction. A shield SH is set to keep the zeroth-order beam (reflected beam) from entering the optical system. The quarter-wave plates Q1 and Q2 prevent the diffraction beams from going back into the LD because each polarization state will be changed by 90° after passing a quarter-wave plate twice. The two diffraction beams are combined at PBS1 and converted into left and right circularly polarized beams by Q3. With the phase shift module composed by a nonpolarizing beam splitter (NPBS), PBS2, and PBS3, the interference fringe with 90° phase shift can be detected by photodetectors PD1 to PD4. Because of the Doppler shift caused by the grating's lateral motion, the diffraction beams will have a phase shift proportional to the motion speed of the grating. When the grating moves a half-pitch ($d/2$), the beat frequency signal has a phase variation of one period (360°). With a holographic grating of 1200 lines/mm, there is a wave cycle of the orthogonal signals at every 416 nm of the grating movement. This process can mathematically be derived as given below.

B. Polarization Analysis

Based on the Jones vector theory, a polarized beam can be described by a two-dimensional vector and the optical component is expressed by a 2×2 transfer matrix. Some common polarizations are listed in Table 1 [22–24].

Letting the grating's diffraction coefficient be $k_P(\theta)$ for the *P* beam and $k_S(\theta)$ for the *S* beam, where θ is the incident angle, the transfer matrix can be defined as

$$M_G = \begin{bmatrix} -k_P(\theta) & 0 \\ 0 & k_S(\theta) \end{bmatrix}. \quad (1)$$

For the left beam, its cascaded transfer matrix of Q1-M1-G-M1-Q1 is

Table 1. Mathematical Expression of Some Typical Polarizations

Polarization	Jones Vector	Optics	Transfer Matrix
Horizontal Polarization	$\begin{bmatrix} 1 \\ 0 \end{bmatrix}$	PBS, horizontally installed	Through: $\begin{bmatrix} 1 & 0 \\ 0 & 0 \end{bmatrix}$ Reflecting: $\begin{bmatrix} 0 & 0 \\ 0 & 1 \end{bmatrix}$
Vertical Polarization	$\begin{bmatrix} 0 \\ 1 \end{bmatrix}$	PBS, with 45° rotation of fast axis	Through: $\frac{1}{2} \begin{bmatrix} 1 & 1 \\ 1 & 1 \end{bmatrix}$ Reflecting: $\frac{1}{2} \begin{bmatrix} 1 & -1 \\ -1 & 1 \end{bmatrix}$
Right Circular Polarization	$\frac{\sqrt{2}}{2} \begin{bmatrix} 1 \\ -i \end{bmatrix}$	1/4 wave plate, fast axis with 45° decline	$\frac{\sqrt{2}}{2} \begin{bmatrix} 1 & i \\ i & 1 \end{bmatrix}$
Left Circular Polarization	$\frac{\sqrt{2}}{2} \begin{bmatrix} 1 \\ i \end{bmatrix}$		

$$M_{Q1-M1-G-M1-G1} = \frac{\sqrt{2}}{2} \begin{bmatrix} 1 & i \\ i & 1 \end{bmatrix} \begin{bmatrix} -k_P(\theta) & 0 \\ 0 & k_S(\theta) \end{bmatrix} \times \frac{\sqrt{2}}{2} \begin{bmatrix} 1 & i \\ i & 1 \end{bmatrix}$$

$$= \frac{1}{2} \begin{bmatrix} -k_P(\theta) - k_S(\theta) & -i(k_P(\theta) - k_S(\theta)) \\ -i(k_P(\theta) - k_S(\theta)) & k_P(\theta) + k_S(\theta) \end{bmatrix} = \frac{1}{2} \begin{bmatrix} -a & -ib \\ -ib & a \end{bmatrix}, \quad (2)$$

where

$$\begin{cases} a = k_P(\theta) + k_S(\theta) \\ b = k_P(\theta) - k_S(\theta) \end{cases}. \quad (3)$$

A similar Jones matrix can be derived for the right beam. The approximate linear polarized beam emitted by the LD can be expressed by $\begin{bmatrix} 1 \\ 1 \end{bmatrix}$. The left and right circular beams propagating from Q3 can thus be derived as

$$E_L = \frac{\sqrt{2}}{2} \begin{bmatrix} 1 & i \\ i & 1 \end{bmatrix} \begin{bmatrix} 1 & 0 \\ 0 & 0 \end{bmatrix} \frac{1}{2} \begin{bmatrix} -a & -ib \\ -ib & a \end{bmatrix} \begin{bmatrix} 0 & 0 \\ 0 & 1 \end{bmatrix} \begin{bmatrix} 1 \\ 1 \end{bmatrix}$$

$$= -\frac{\sqrt{2}bi}{4} \begin{bmatrix} 1 \\ i \end{bmatrix}, \quad (4)$$

$$E_R = \frac{\sqrt{2}}{2} \begin{bmatrix} 1 & i \\ i & 1 \end{bmatrix} \begin{bmatrix} 0 & 0 \\ 0 & 1 \end{bmatrix} \frac{1}{2} \begin{bmatrix} -a & -ib \\ -ib & a \end{bmatrix} \begin{bmatrix} 1 & 0 \\ 0 & 0 \end{bmatrix} \begin{bmatrix} 1 \\ 1 \end{bmatrix}$$

$$= \frac{\sqrt{2}b}{4} \begin{bmatrix} 1 \\ -i \end{bmatrix}. \quad (5)$$

Therefore, after passing through Q3, the two beams are all circularly polarized.

C. Phase Analysis

When a beam with original frequency f_0 propagates into a moving grating, the frequency shift causing the beat interference is determined by the Doppler effect and the diffraction law [23–26]

$$\begin{cases} \Delta f = f_0 \frac{v}{c} (\sin \theta_i + \sin \theta_q) \\ d(\sin \theta_i + \sin \theta_q) = m\lambda \\ c = \lambda f_0 \end{cases}. \quad (6)$$

The parameters in Eq. (6) are defined as below:

v , grating velocity;
 c , light speed in vacuum;
 θ_i , incident angle;
 θ_q , diffraction angles;
 $d = 1/1200$, grating constant; and
 $m = \pm 1$, diffraction order.
 Then frequency shift is simplified as

$$\Delta f = m \frac{v}{d} = \pm \frac{v}{d}, \quad (7)$$

$$\Delta \omega = 2\pi \Delta f = \pm 2\pi \frac{v}{d}. \quad (8)$$

Therefore, after passing through Q3, the electric field vectors of the circularly polarized left and right beams are

$$\vec{E}_L = A \cdot \exp[i(\omega - \Delta\omega)t] \begin{bmatrix} 1 \\ i \end{bmatrix}, \quad (9)$$

$$\vec{E}_R = A \cdot \exp[i(\omega + \Delta\omega)t] \begin{bmatrix} 1 \\ -i \end{bmatrix}. \quad (10)$$

The electric fields of the beams on four photo-detectors are

$$\vec{E}_{PD1} = \begin{bmatrix} 0 & 0 \\ 0 & 1 \end{bmatrix} (\vec{E}_L + \vec{E}_R)$$

$$= \begin{bmatrix} 0 \\ 1 \end{bmatrix} 2A \exp(i\omega t) \sin(\Delta\omega \cdot t), \quad (11)$$

$$\vec{E}_{PD2} = \begin{bmatrix} 1 & 0 \\ 0 & 0 \end{bmatrix} (\vec{E}_L + \vec{E}_R)$$

$$= \begin{bmatrix} 1 \\ 0 \end{bmatrix} 2A \exp(i\omega t) \cos(\Delta\omega \cdot t), \quad (12)$$

$$\vec{E}_{PD3} = \frac{1}{2} \begin{bmatrix} 1 & 1 \\ 1 & 1 \end{bmatrix} (\vec{E}_L + \vec{E}_R)$$

$$= \begin{bmatrix} 1 \\ 1 \end{bmatrix} A \exp(i\omega t) [\cos(\Delta\omega \cdot t) + \sin(\Delta\omega \cdot t)], \quad (13)$$

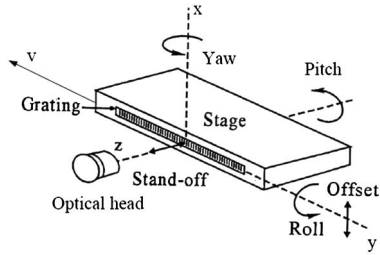


Fig. 2. Typical geometric errors.

$$\begin{aligned} \vec{E}_{PD4} &= \frac{1}{2} \begin{bmatrix} 1 & -1 \\ -1 & 1 \end{bmatrix} (\vec{E}_L + \vec{E}_R) \\ &= \begin{bmatrix} 1 \\ 1 \end{bmatrix} A \exp(i\omega t) [\cos(\Delta\omega \cdot t) - \sin(\Delta\omega \cdot t)]. \end{aligned} \quad (14)$$

Substituting Eq. (8) into Eqs. (11)–(14), the light intensity on each photodetector can be obtained as

$$\begin{aligned} I_{PD1} &= \|\vec{E}_{PD1}\|^2 = A[1 - \cos(2\Delta\omega \cdot t)] \\ &= A \left[1 - \cos\left(2\pi \cdot \frac{2v}{d} \cdot t\right) \right] = A \left[1 - \cos\left(2\pi \cdot \frac{2s}{d}\right) \right], \end{aligned} \quad (15)$$

$$\begin{aligned} I_{PD2} &= \|\vec{E}_{PD2}\|^2 = A[1 + \cos(2\Delta\omega \cdot t)] \\ &= A \left[1 + \cos\left(2\pi \cdot \frac{2v}{d} \cdot t\right) \right] \\ &= A \left[1 + \cos\left(2\pi \cdot \frac{2s}{d}\right) \right], \end{aligned} \quad (16)$$

$$\begin{aligned} I_{PD3} &= \|\vec{E}_{PD3}\|^2 = A[1 + \sin(2\Delta\omega \cdot t)] \\ &= A \left[1 + \sin\left(2\pi \cdot \frac{2v}{d} \cdot t\right) \right] \\ &= A \left[1 + \sin\left(2\pi \cdot \frac{2s}{d}\right) \right], \end{aligned} \quad (17)$$

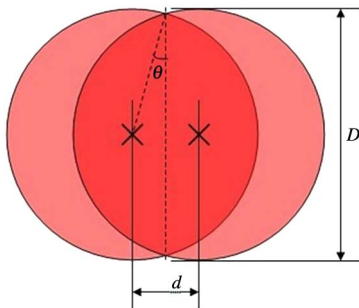


Fig. 3. (Color online) Interfering spots.

Table 2. Spots Moving Situation and Tolerance

Geometric Errors	Spots Movement on the Photodetector	Tolerance (10% intensity loss)
Yaw		—
Roll		—
Pitch		0.15°
Standoff		—
Offset		—

$$\begin{aligned} I_{PD4} &= \|\vec{E}_{PD4}\|^2 = A[1 - \sin(2\Delta\omega \cdot t)] \\ &= A \left[1 - \sin\left(2\pi \cdot \frac{2v}{d} \cdot t\right) \right] = A \left[1 - \sin\left(2\pi \cdot \frac{2s}{d}\right) \right]. \end{aligned} \quad (18)$$

It is clearly seen that the signal's phase is encoded by the instantaneous displacement ($s = vt$). With differential input, the DC offset can be effectively decreased.

An advantage of this new system design is that compared with our earlier systems [15,16] using 14 optics and [23] using 12 optics, this system is only constructed with 11 optics including the additional shield plate. It will be explained in Section 4 that more optics means a more difficult bonding process.

3. Principle of Compact LDGI

The typical geometric errors of the proposed system are shown in Fig. 2. During the movement, there will be angular errors, called yaw, pitch, and roll, and linear errors, called standoff and offset.

The signal contrast will be weakened by spots separations caused by geometrical errors. As shown in Fig. 3, only the overlapping area produces interferences while the others only contribute to the DC offset. Accordingly, the signal intensity of the

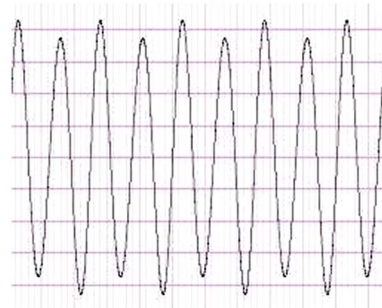


Fig. 4. (Color online) Harmonic disturbance caused by redundant reflections.

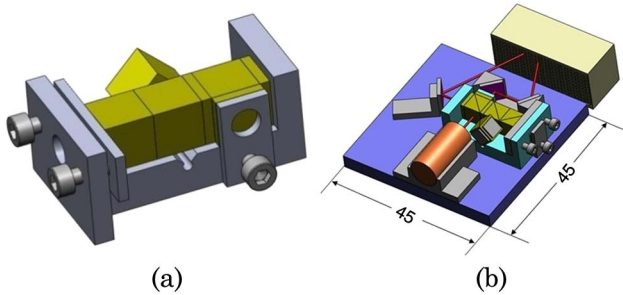


Fig. 5. (Color online) Compact LDGI system bonded with a mechanical fixture. (a) Optics in clamping; (b) actual dimensions (in mm).

interference beam is proportional to the overlapping area. Compared to the ideal signal, the intensity ratio with tolerance can be expressed by

$$C = \frac{S1}{S2} = \frac{\pi r^2 \cdot \frac{\pi - 2\theta}{2\pi} \times 2 - r^2 \sin 2\theta}{\pi r^2} \times 100\%, \quad (19)$$

where $S1$ denotes the overlapping area shown in Fig. 3, $S2$ is the ideal area, and

$$\theta = \arcsin \frac{d}{2r}. \quad (20)$$

It is easily seen that the grating is insensitive to an offset as long as the light is projected onto the grating. Besides, since the diffraction angles are equal to the incident angles, this system is immune to standoff.

The influence of angular errors can be analyzed by LightTools. From Eq. (19), the tolerance of each geometrical error can be calculated with a given intensity loss. The situations of spots separations with respect to each geometrical error are listed in Table 2. The tolerance limit is given when the intensity ratio is at 90%. It is seen that the offset and standoff do not alter the spots, and yaw and roll errors do not change the intensity because the spots move simultaneously. A normal linear stage will have pitch errors of up to a few arc seconds only. Therefore, this improved LDGI is almost immune to geometric errors.

4. Compact Design

The air gap between two contacting surfaces will cause unexpected reflections resulting in some ghost spots. If any ghost spot emits to the grating, harmonic disturbance will be generated, causing alternately changing amplitudes of the interference signals, as shown in Fig. 4. This is very likely to happen when too many optics are bonded together with adhesive glue [15,16].

From the optical configuration of the LDGI system shown in Fig. 1, it is seen that five optics (Q1, PBS1, Q3, NPBS, and PBS2) can be lined up. An innovative mechanical clamping fixture is, therefore, designed to firmly press these five parts together with setting screws, as shown in Fig. 5(a). An elastic pad is inserted in the end of the fixture to absorb redundant pressing force. This new idea of mechanical bonding

technique is simple and an air gap will definitely not occur. In addition, the same procedure can easily be reproduced by anyone without the need of a skillful technician. The clamping force is applied through an adjustable plate to the optics. The deformation of optics can be minimized with carefully controlled screwing force. Moreover, since human-induced adhesive errors are entirely avoided by this process, all optical components can be selected to the smallest size in order to make the system as compact as possible. Figure 5(b) shows that the developed LDGI system is of about the same scale as the grating. This is especially useful when the linear stage is small.

5. Signal Normalization and Subdivision

Typical waveform signal distortions of motion sensors are DC drift, amplitude variation, and phase error [20]. The usual Lissajous circle may become a tilted ellipse, as shown in Fig. 6.

In our previous design, a software-based correction scheme was employed to compensate for the distortion errors [21]. The real-time performance, however, is subject to the computational workload. In this study, the signal processing is mostly conducted by a specially designed electronic circuit in which the DC offset and amplitude difference are normalized by adjusting the floating reference and amplifying the scale. Besides, the influence of amplitude variation can be eliminated by the division operation during the process of phase subdivision [21]. Then the phase error is corrected by vector summation and subtraction operations as follows.

Suppose the two nonorthogonal waveforms are $X = u(x) = \sin(x)$ and $Y = v(x) = \sin(x + \varphi)$, where $\varphi \neq 0$. The outputs can then be configured as

$$\begin{aligned} u'(x) &= u(x) + v(x) = \sin(x) + \sin(x + \varphi) \\ &= 2 \sin \frac{2x + \varphi}{2} \cos \frac{\varphi}{2}, \end{aligned} \quad (21)$$

$$\begin{aligned} v'(x) &= u(x) - v(x) = \sin(x) - \sin(x + \varphi) \\ &= 2 \cos \frac{2x + \varphi}{2} \sin \frac{\varphi}{2}. \end{aligned} \quad (22)$$

Thus, the newly configured waveforms $u'(x)$ and $v'(x)$ have an exact phase shift of 90° . The Lissajous circles before and after vector operations are shown in Fig. 7.

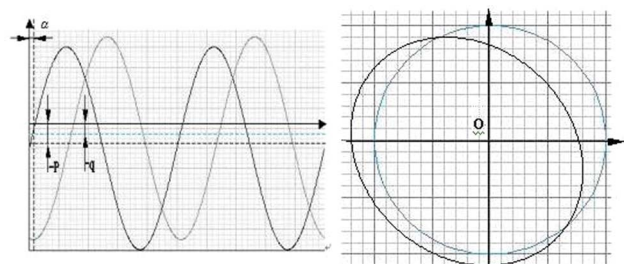


Fig. 6. (Color online) Typical signal distortions.

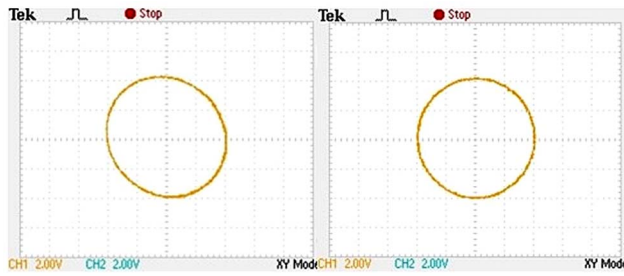


Fig. 7. (Color online) Lissajous signals before (left) and after (right) vector operations.

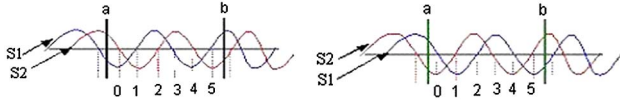


Fig. 8. (Color online) Pulse counting in forward (left) and reverse (right) motions.

The corrected waveform signals can then be used for the software-based pulse counting and period subdivision down to the level of nanometer resolution. Since the sign of the phase shift, positive or negative, has an apparent relationship with the moving direction (shown in Fig. 8), the pulse-counting algorithm is based on the following rules:

if S1 crosses zero from negative to positive while S2 is negative, count +1, else count -1;

if S1 crosses zero from positive to negative while S2 is positive, count +1, else count -1;

if S2 crosses zero from negative to positive while S1 is positive, count +1, else count -1;

if S2 crosses zero from positive to negative while S1 is negative, count +1, else count -1.

This algorithm is deemed more robust than the conventional counting using a given threshold value of the signal intensity, which is also called a DC counting. It is known that when the signal variation occurs due to geometric errors of the moving stage, it may cause missing counts. The proposed counting method is based on the number of zero crossings, being a kind of AC counting, which is free from amplitude variations of the sampled signals. As shown in Fig. 9, even if there is micronoise in the signal (exaggerated in the figure), the net algebraic count is the same as the up and down fluctuations and can compensate each other.

The pulse-counting procedure only calculates the integer numbers of the quarter-pitch. The resolution is still limited to 104 nm. For less than a quarter-pitch motion, a subdivision method has to be applied. Since this is done by software in the developed system, a general lookup table (LUT) of tangent data is stored for this purpose. If the LUT stores data of every one degree of phase, the resolution of the signal subdivision can easily reach less than 1 nm without any difficulty.

6. Experimental Test

The developed LDGI system, together with the signal processing circuit and the displacement subdivision software, was verified by experiments with five

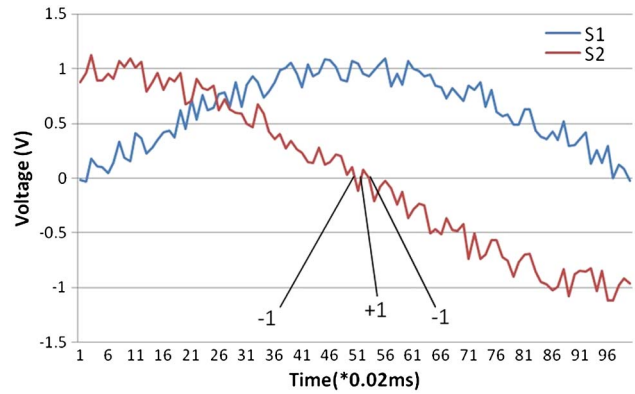


Fig. 9. (Color online) Noise-immune principle.

Table 3. Experimental Data of Displacement Measurements

Position (mm)	0.1	1	5	10	15
Error 1 (nm)	1	96	432	882	1315
Error 2 (nm)	2	105	421	881	1338
Error 3 (nm)	-1	88	439	861	1332
Error 4 (nm)	0	87	418	875	1321
Error 5 (nm)	3	99	425	876	1329
Average Error (nm)	1	95	427	877	1327
Standard deviation (nm)	1.6	7.6	8.5	8.0	9.1

Table 4. Experimental Data after the Third-Order Polynomial Correction

Position (mm)	0.1	1	5	10	15
Error 1 (nm)	-7	11	0	7	-12
Error 2 (nm)	-6	20	-11	6	11
Error 3 (nm)	-9	3	7	-14	5
Error 4 (nm)	-8	2	-14	0	-6
Error 5 (nm)	-5	14	-7	1	2
Average Error (nm)	-7	10	-5	2	0

different displacements of approximately 0.1 mm, 1 mm, 5 mm, 10 mm, and 15 mm. Each experiment was repeated five times. The results of the LDGI readings were compared with the actual displacement read by the HP5529A laser interferometer and the errors were recorded. Table 3 lists the experimental results.

A trend of progressive errors can easily be seen in Table 3 due to many influence factors; for instance, the imperfect alignment of the laser beam to the motion axis of the stage is likely to yield a cosine error. Besides, the systematic straightness error of the moving stage as well as the permanent distortion of the grating while mounting may contribute to high-order components of the error curve. A third-order polynomial fit to the systematic error is conducted:

$$d_c = 0.19x^3 - 3.59x^2 + 100.22x - 6.04. \quad (23)$$

The residual errors after the error correction are mostly due to random errors, as listed in Table 4. Combining the results from Tables 3 and 4, it is verified that the accuracies and standard deviations of

the developed LDGI are all less than 10 nm for stroke lengths up to 15 mm.

7. Conclusions

In this paper, the design and work model of a high-precision displacement sensor named LDGI is presented for long-range and high-resolution measurements. With a simplified structure, the alignment head-to-scale tolerance can be significantly enhanced. A hardware-based signal processing circuit and a software-based waveform counting and signal subdivision algorithm are developed for a real-time displacement recording. Some special features of this system are:

1. simplified structure with less components and higher tolerance. It is very suitable for a displacement sensing of fine motion stages,
2. less number of optics compared with our precious designs,
3. mechanical fixture for optical bonding without an air gap and easily reproducible,
4. real-time signal processing and correction by hybrid hardware/software implementation,
5. high head-to-scale assembly tolerance, and
6. high accuracy and repeatability.

The work reported is a part of an International Cooperation Project founded by the National Natural Science Foundation of China (NSFC) under contract number 50420120134.

References

1. X. H. Chen, Y. Zhao, and D. C. Li, "Review on optical nanometrology," *Opt. Tech.* **3**, 74–78 (1999).
2. J. A. Cramar, "Nanometer resolution metrology with the molecular measuring machine," *Meas. Sci. Technol.* **16**, 2121–2128 (2005).
3. N. Bobroff, "Recent advances in displacement measuring interferometry," *Meas. Sci. Technol.* **4**, 907–926 (1993).
4. T. Pozar, P. Gregorcic, and J. Mozina, "Optimization of displacement-measuring quadrature interferometers considering the real properties of optical components," *Appl. Opt.* **50**, 1210–1219 (2011).
5. F. M. Gerasimov, "Use of diffraction gratings for controlling of a ruling engine," *Appl. Opt.* **6**, 1861–1865 (1967).
6. M. L. Schattenburg and H. I. Smith, "The critical role of metrology in nanotechnology," *Proc. SPIE* **4608**, 116–124 (2002).
7. C. L. Chu and K. C. Fan, "Design of a digital controller for long-stroke submicron positioning stage," in *Proceedings of the 1st International Conference of Positioning Technology (ICPT, 2004)*, pp. 176–181.
8. S. G. Rautian, "On the theory of interferometers with diffraction gratings," *Opt. Spectrosc.* **93**, 934–940 (2002).
9. A. Kozłowska, M. Kujawińska, and C. Gorecki, "Grating interferometry with a semiconductor light source," *Appl. Opt.* **36**, 8116–8120 (1997).
10. X. C. Chu, H. B. Lü, and S. H. Zhao, "Research on long-range grating interferometry with nanometer resolution," *Meas. Sci. Technol.* **19**, 017001 (2008).
11. K. C. Fan and C. D. Su, "Error analysis for a diffraction grating interferometric stylus probing system," *Meas. Sci. Technol.* **12**, 482–490 (2001).
12. K. C. Fan and Y. S. Liu, "A linear diffraction grating interferometer with high accuracy," *Proc. SPIE* **6280**, 628008 (2006).
13. Y. Jourlin, J. Jay, and O. Parriaux, "Compact diffractive interferometric displacement sensor in reflection," *Precis. Eng.* **26**, 1–6 (2002).
14. K. W. Wang and L. J. Zeng, "Double-grating frequency shifter for low-coherence heterodyne interferometry," *Opt. Commun.* **251**, 1–5 (2005).
15. K. C. Fan and Z. F. Lai, "A displacement spindle in a micro/nano level," *Meas. Sci. Technol.* **18**, 1710–1717 (2007).
16. C. F. Kao, S. H. Lu, H. M. Shen, and K. C. Fan, "Diffractive laser encoder with a grating in Littrow configuration," *Jpn. J. Appl. Phys.* **47**, 1833–1837 (2008).
17. P. Wen and D. H. Hsu, "Direct subdivision of moiré fringe with CCD," *Proc. SPIE* **1230**, 165–166 (1990).
18. J. Cui, H. Q. Li, and Q. Chen, "New digital subdividing and raster-sensing technique for moiré fringe and gratings," *Opt. Tech.* **26**, 294–296 (2000).
19. K. C. Fan and Y. J. Chen, "A study on digital subdivision of linear optical encoder for nanopositioning," in *Proceedings of the 6th International Conference on Frontiers of Design and Manufacturing* (Science Press, 2004).
20. K. P. Birch, "Optical fringe subdivision with nanometric accuracy," *Precis. Eng.* **12**, 195–198 (1990).
21. K. C. Fan and F. Cheng, "Nanopositioning control on a commercial linear stage by software error correction," *Nanotech. Precis. Eng.* **4**, 1–9 (2006).
22. R. Guenther, *Modern Optics* (Wiley, 1990).
23. K. C. Fan, B. K. Li, and C. H. Liu, "A diffraction grating scale for long range and nanometer resolution," *Proc. SPIE* **7133**, J1–J8 (2009).
24. F. Cheng, "Study on the key technology of nano-CMM measurement and control system," Ph.D. thesis (Hefei University of Technology, 2010).
25. F. L. Petrotti and L. S. Petrotti, *Introduction to Optics*, 2nd ed. (Prentice-Hall, 1996).
26. E. Hecht, *Optics* (Addison-Wesley, 1998).